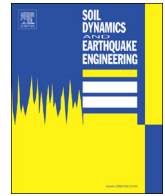




ELSEVIER

Contents lists available at ScienceDirect

## Soil Dynamics and Earthquake Engineering

journal homepage: [www.elsevier.com/locate/soildyn](http://www.elsevier.com/locate/soildyn)

## Liquefaction-induced settlement and tilting of buildings with shallow foundations based on field and laboratory observation

Kohji Tokimatsu<sup>a,\*</sup>, Kazuya Hino<sup>b</sup>, Hiroko Suzuki<sup>c</sup>, Kyoko Ohno<sup>d</sup>, Shuji Tamura<sup>d</sup>, Yasutsugu Suzuki<sup>e</sup>

<sup>a</sup> Tokyo Soil Research, Co. Ltd., 2-11-16 Higashigaoka, Meguro-ku, Tokyo 152-0021, Japan

<sup>b</sup> Electric Power Development Co., Ltd., Tokyo, Japan

<sup>c</sup> Chiba Institute of Technology, Chiba, Japan

<sup>d</sup> Tokyo Institute of Technology, Tokyo, Japan

<sup>e</sup> Kajima Technical Research Institute, Chofu, Tokyo, Japan

## ARTICLE INFO

## Keywords:

Liquefaction

Settlement

Tilting

Building

Shallow foundation

Case history

Centrifuge test

## ABSTRACT

In order to examine relative importance of key parameters affecting liquefaction-induced settlement and tilting of buildings with shallow foundations, earthquake reconnaissance studies and centrifuge experiments were made and their results were compared with those of similar previous studies. It is shown that: (1) The liquefaction-induced relative settlement and tilting of shallow foundations tend to increase with increasing contact pressure and ground settlement, and with decreasing groundwater table depth and thickness of the non-liquefied crust; (2) The tilt angle of the building also tends to increase with increasing eccentric mass and distance ratio; and (3) The safety factors against vertical load and dynamic overturning moment are key indicators to estimate liquefaction-induced damage to buildings with rigid shallow foundations.

### 1. Introduction

During the 2011 Tohoku Earthquakes, extensive soil liquefaction occurred in many reclaimed lands of the Tokyo Bay area and along the Tone River basin, causing excessive settlement and tilting of many residential wooden houses and low-rise reinforced concrete (RC) buildings founded on shallow foundations. Similar damage to residential houses was also observed not only on reclaimed lands but also on natural deposits during recent earthquakes such as the 2011 Christchurch and 2016 Kumamoto earthquakes. Despite many reconnaissance and laboratory studies on soil liquefaction (e.g., [3,6,8,9,11,13,14]), the various factors and their effects leading to settlement of buildings with shallow foundations have not been thoroughly understood to date. In addition, most of the previous studies concentrated only on building settlement, overlooking building tilt failure which is equally or even more important when considering the serviceability of the building after the quake, i.e., performance-based seismic design of buildings with shallow foundations. The objective of this paper is therefore to examine relative importance of key parameters affecting not only settlement but also tilting of buildings with shallow foundations founded on liquefiable soils based on both field observation and laboratory experiments.

### 2. Field observation

#### 2.1. Field observation of past earthquakes

Fig. 1 schematically illustrates key factors controlling liquefaction-induced settlement and tilt,  $S$  and  $\theta$ , of a building, which were observed in past reconnaissance studies. These factors can be classified into three categories, i. e., building, ground and earthquake conditions. Based on the field case histories regarding the 1964 Niigata earthquake and 1G shaking table tests, Yoshimi and Tokimatsu [14] showed that the settlement ratio normalized with respect to the thickness of liquefied layer,  $S/D$ , of RC building decreases as the ratio between building width and thickness of liquefied layer,  $B/D$ , increases. Ishihara [6] suggested after the 1983 Nihonkai-Chubu earthquake that, a non-liquefied crust overlying a liquefied deposit,  $D_{NL}$  shown in Fig. 1, if exceeding 2–3 m, would reduce liquefaction-induced damage to wooden houses during earthquakes with peak ground accelerations of less than about  $2 \text{ m/s}^2$ . Tokimatsu et al. [9] postulated that the contact pressure and shear stress imposed by a building as well as proximity to nearby buildings might have affected settlement and tilting of the building based on findings from the 1990 Luzon Earthquake. In more recent studies, Sancio et al. [8] observed that the settlement ratio normalized with

\* Corresponding author.

E-mail address: [tokimatsu@tokyosoil.co.jp](mailto:tokimatsu@tokyosoil.co.jp) (K. Tokimatsu).

<https://doi.org/10.1016/j.soildyn.2018.04.054>

Received 22 January 2018; Received in revised form 24 April 2018; Accepted 27 April 2018  
0267-7261/ © 2018 Elsevier Ltd. All rights reserved.

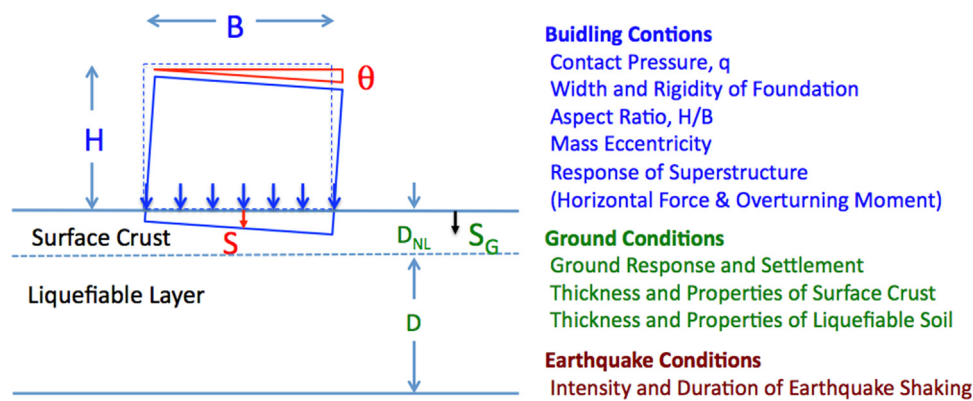


Fig. 1. Key factors controlling liquefaction-induced settlement and tilt of building.

respect to foundation width,  $S/B$ , has a good correlation with the aspect ratio,  $H/B$ , of RC buildings of 4- to 6-story in the 1999 Kocaeli earthquake. Based on reconnaissance studies following the 2011 Tohoku earthquakes, Tokimatsu et al. [10] added that the tilting angles of a wooden house tends to increase with increasing liquefaction-induced ground settlement ( $S_G$ ) around the building, which is in turn influenced by relative density and thickness of the liquefied layer as well as intensity and duration of earthquake ground motions.

Specific factors were often highlighted in these studies, falling short of a more holistic evaluation to determine their cumulative or relative importance to one factor to another. In addition, building tilt failures were hardly discussed which undermine serviceability far more significantly than building settlement, posing a knowledge gap to be addressed.

## 2.2. Field observation during 2016 Kumamoto Earthquakes

The 2016 Kumamoto Earthquakes, consisting of two major events on April 14th and 16th ( $M_w$ 5.8 and  $M_w$ 7.0), induced catastrophic damage to infrastructures and buildings in the source region as well as the Kumamoto plain. The quakes also caused soil liquefaction and related damage, particularly following the second event. Fig. 2 shows typical damage to a 2-story wooden house.

The peak ground accelerations recorded at K-NET in the Kumamoto plain were  $4.24 \text{ m/s}^2$  and  $8.51 \text{ m/s}^2$  for the first and second events, respectively. Despite very strong shaking, the area of soil liquefaction was very limited. This motivates the authors to investigate the reason for such observations and accompanying liquefaction-induced damage. It is also interesting to determine how buildings with shallow foundations behaved under such strong shaking event.

Fig. 3 shows a map of the investigated area encircled by dash line, i.e., Karikusa town and its vicinity located on the south of JR Nishi



Fig. 2. Liquefaction-induced tilt of a 2-story wooden house in Karikusa town.

(West)-Kumamoto station. According to a geomorphological map, most of the area were classified as natural levees presumably consisting of predominantly sandy soil. A total of 307 buildings on spread foundation were examined. Table 1 summarizes the structural type and the number of story of these buildings with occurrence or non-occurrence of soil liquefaction. About 70% are lightweight two story wooden houses. Fig. 3 illustrates the distribution of relative settlement of buildings in the district.

Figs. 4 and 5 show similar distribution of tilt angle and damage level of superstructure of buildings, which have been classified according to Tables 2 and 3. Note that any house inclined more than  $6/1000$ , even without any structural damage, generally requires re-leveling for subsequent usage. From Figs. 3 and 4, it is evident that liquefaction-induced settlement and tilting of buildings were concentrated within a narrow band along the road running from the northeast to the south, which was reportedly an old river channel about 400 years ago and artificially reclaimed sometime in the Edo era (1603–1868). Fig. 4 also indicates that liquefaction-induced settlement of buildings was relatively minor, probably attributed to the fact that most of those buildings were lightweight wooden houses.

Fig. 5 suggests that significant damage to superstructure of buildings were largely distributed on the southeastern part of the investigated area outside of the liquefied belt, indicating significant effects of strong ground shaking amplified through the non-liquefied soil near the ground surface. A few buildings also experienced damage to their superstructures in the southern part of the liquefied belt. During the survey, it was observed that all these buildings were very old wooden houses with unreinforced weak foundations. Therefore, it is expected that the occurrence of soil liquefaction would result in unacceptable deformation to their superstructures. This reflects the historical changes in design specification of continuous foundation of wooden houses, in which more reinforcements were stipulated over time, following important lessons learned from performances of geotechnical structures in the last half century [12].

Cone penetration tests were conducted at five locations (S1 to S5) across the old river channel, along with standard penetration tests at two sites (S3 and S5). Sites S2–S4 were located inside the liquefied belt, while Sites S1 and S5 were outside as shown in Figs. 4–6. Fig. 6 shows the distribution of cone tip resistance and normalized soil behavior type index ( $I_c$ ) with depth of the five sites. Although all sites are located within the natural levees classified in the geomorphological chart of the region, sandy soils with  $I_c < 2$  dominate from the ground surface to a depth of about 6 m at liquefied sites S2 to S4, while silty and clayey soils with  $I_c > 2$  prevail within the same depth at non-liquefied sites S1 and S5. This suggests that the difference in liquefaction-induced damage in the region could be attributed to the differences in near surface soil type.

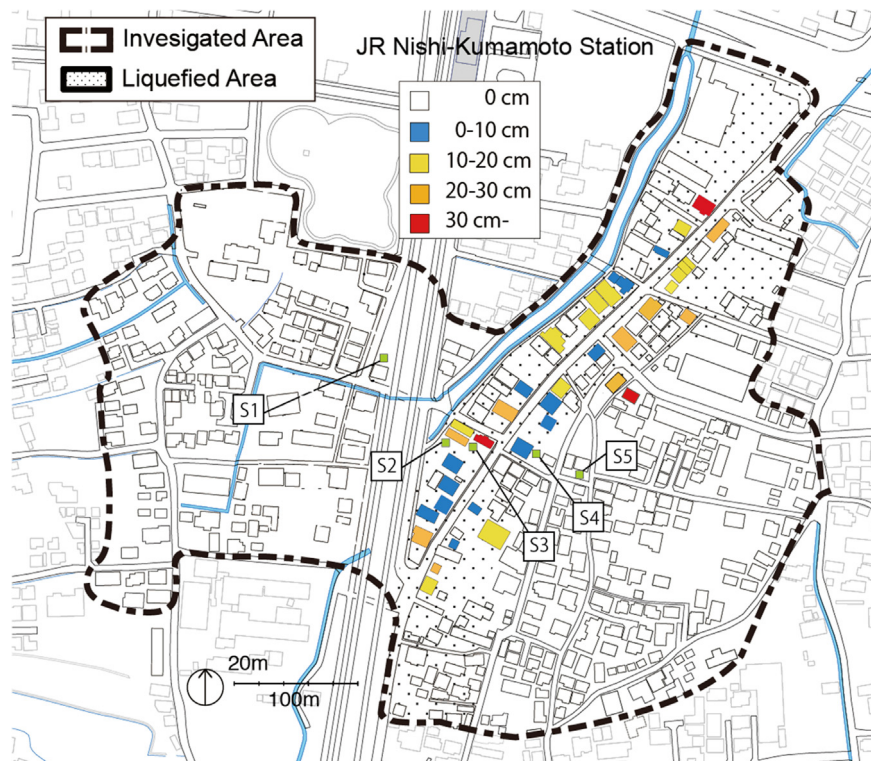


Fig. 3. Distribution of liquefaction-induced settlement of buildings in Karikusa town.

Table 1

Number of stories and structural type of buildings investigated with sign of soil liquefaction.

Type of structure	No. of story	Liquefaction		Total
		Yes	No	
W	1	4	66	70
	2	18	75	93
S	1	0	9	9
	2	21	83	104
	3	5	6	11
RC	1	2	0	2
	2	2	9	10
	3	3	3	6
	4	0	1	1
	5	0	1	1
Total		54	253	307

### 2.3. Revisit to field case histories of liquefaction-induced damage to buildings

Previous studies on liquefaction-induced damage to buildings during past three catastrophic earthquakes are revisited along with those observed in the Kumamoto region to identify, if any, the differences in damage patterns between these earthquakes, and to explore key parameters influencing the trends of damage observed. The past case histories analyzed in conjunction with the Kumamoto data, include those in Niigata during the 1964 Niigata earthquake [14], Dagupan during the 1990 Luzon earthquake [9], and Adapazari during the 1999 Kocaeli earthquake [8,13].

Table 4 summarizes the statistics of maximum settlement relative to the ground and tilt angle of buildings observed in the four earthquakes. The maximum relative building settlement and tilting in the Kumamoto earthquakes were less than 40 cm and 1/20, which are significantly less than those observed in any of the other earthquakes. This could be due to that most of the buildings in the Karikusa town are lightweight two

story wooden houses, whereas most are three- to five-story reinforced concrete buildings in other cases.

Fig. 7 shows the relation between average relative settlement and number of stories or aspect ratio of each building from the four events. Note that unlike the previous study [12], the ordinate of the figure has been replaced from the maximum to the average relative settlement. There are general trends observed: (1) the average relative settlement of building in each of the four events tends to increase with increasing number of stories and aspect ratio but (2) the data from Niigata generally falls on the upper bound while those from Adapazari and Kumamoto fall near the lower bound. Data from Dagupan are located in between. Such a site-specific trend is likely due to the differences in soil conditions such as the thickness, density and soil type of liquefied sand between these cities.

Following up on the discussion of Fig. 7, the relative settlement was normalized with respect to foundation width and thickness of the liquefied layer (B and D shown in Fig. 1), each herein defined as settlement-width ratio (S/B) and settlement-thickness ratio (S/D), respectively. Figs. 8 and 9 show their relations with number of stories and aspect ratio of building. The site-specific scatter trend shown in Fig. 7 has diminished particularly when the settlement was normalized with respect to the thickness of liquefied layer as shown in Fig. 9. It is however, noted that the denominator of the vertical axis, D in Fig. 9, was estimated and thus less certain than B in Fig. 8.

Fig. 10 shows the building tilt angle with the number of stories and aspect ratio of building for all cases. A general trend is observed where the tilt angle of building tends to increase with larger number of stories and aspect ratio, while site-specific trend observed in Fig. 7 is less obvious. The figure also suggests that the large tilt leading to overturning instability occurred only for buildings over 3 stories high and an aspect ratio exceeding about 2. Similar field observation regarding overturning conditions of buildings was also reported elsewhere [4].

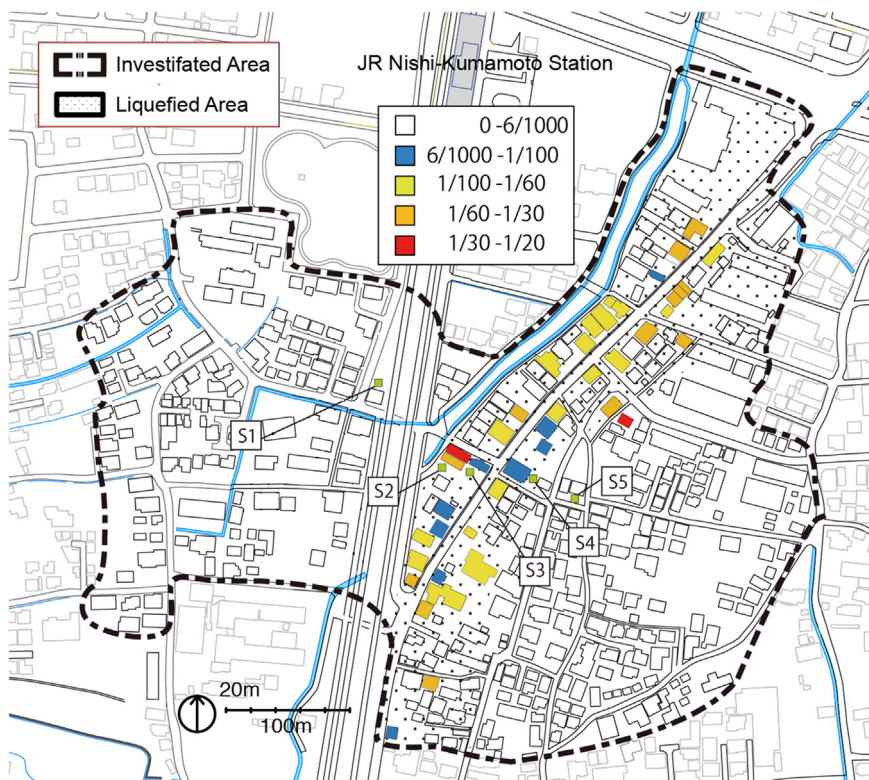


Fig. 4. Distribution of liquefaction-induced tilt of buildings in Karikusa town.

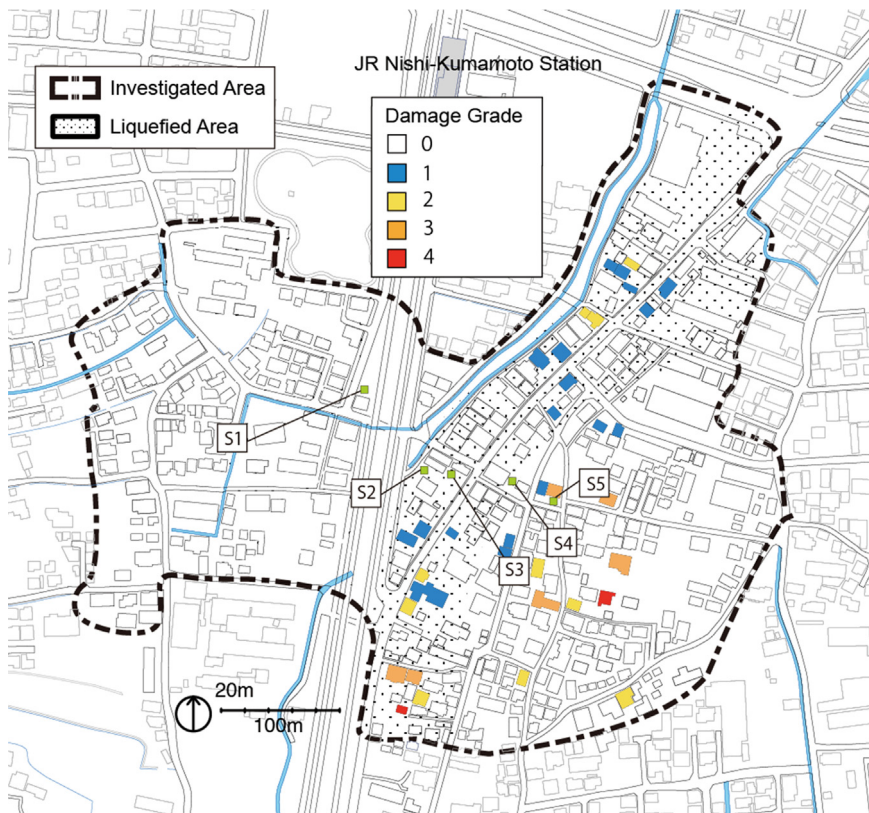


Fig. 5. Distribution of damage to superstructure of buildings in Karikusa town.

**Table 2**  
Relation of tilt angle of building with health problem, degree of damage, and need for restoration.

Tilt angle (Rad)	Health problem [1]	Degree of damage [2]	Need for restoration without health problems
6/1000	Strong feeling of inclination		Likely
1/100	Disorders such as dizziness and headache	Partially damaged	Definitely
1/60	Physiological limit	Largely damaged	
1/20		Totally damaged	

**Table 3**  
Classification of damage to buildings (After [7,13]).

Damage grade	Description
0	No damage
1	Negligible to slight damage
2	Moderate damage
3	Substantial to heavy damage
4	Very heavy damage
5	Destruction

**Table 4**  
Statistics of liquefaction-induced damage to building used from case histories in four earthquakes.

Settlement (cm)	Number of buildings			
	1964 Niigata	1990 Luzon	1999 Kocaeli	2016 Kumamoto
0-1	0	7	14	7
1-20	5	2	29	34
20-40	5	6	20	13
40-60	1	7	9	0
60-	21	35	1	0

Tilt Angle (rad)	Number of buildings			
	1964 Niigata	1990 Luzon	1999 Kocaeli	2016 Kumamoto
0-6/1000	2	8	13	14
6-10/1000	4	5	2	5
1/100-1/60	4	1	0	16
1/60-1/20	5	26	40	19
1/20-	17	17	18	0

Number of Stories	Number of buildings			
	1964 Niigata	1990 Luzon	1999 Kocaeli	2016 Kumamoto
1	1	0	4	6
2	6	6	7	40
3	14	23	15	8
4	10	17	17	0
5	1	11	26	0
6	0	0	6	0

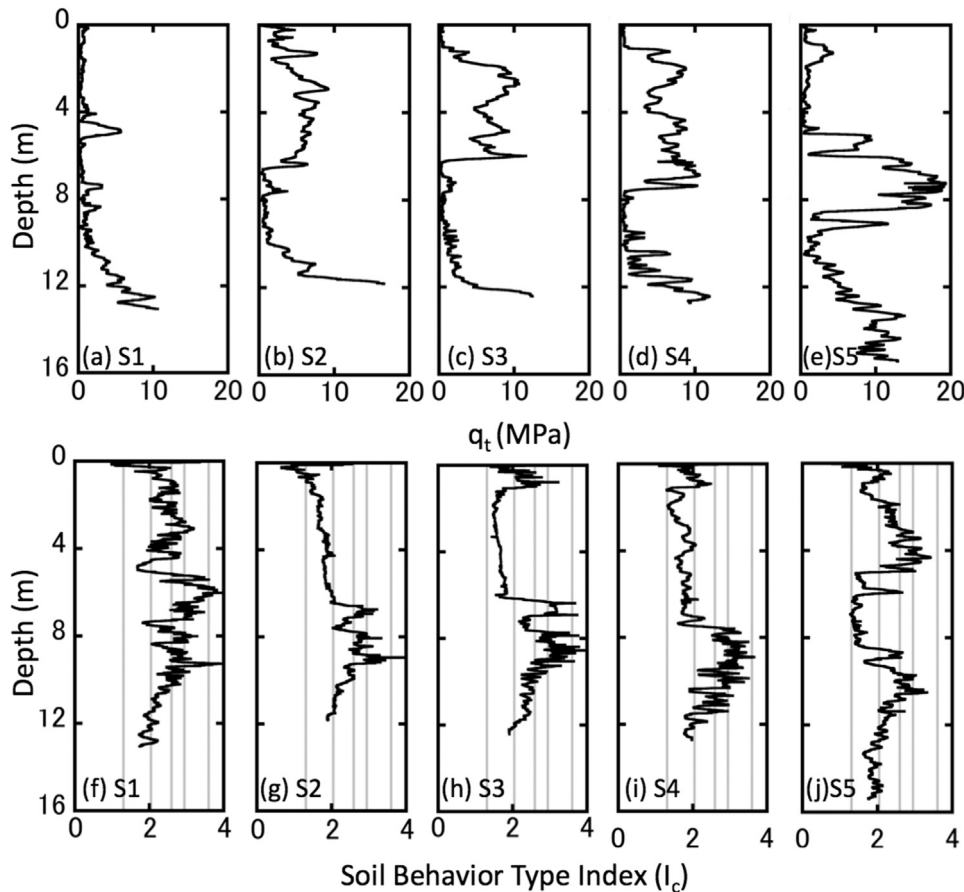


Fig. 6. CPT tip resistance and soil behavior type index ( $I_c$ ) at Sites 1-5.

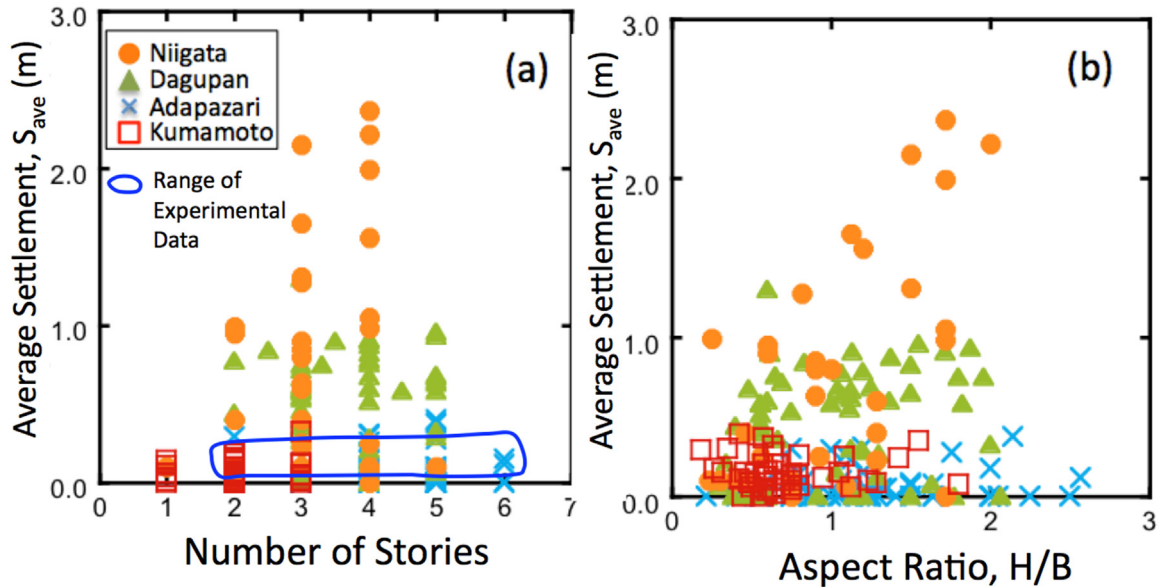


Fig. 7. Relation of average relative settlement with number of stories and aspect ratio of building.

### 3. Observations from laboratory experiments

#### 3.1. Laboratory observations from past centrifuge experiments

Dashti et al. [3] conducted centrifuge experiments simulating the performance of reinforced concrete (RC) buildings in liquefiable soils and suggested that the key factors controlling liquefaction-induced building settlement are seismic demand, liquefaction layer thickness (D), foundation width (B), static shear stress ratio, building aspect ratio (H/B), foundation contact pressure ( $q$ ), and 3D drainage. Combining various building and soil conditions, more comprehensive centrifuge liquefaction experiments have been conducted recently (e.g., [11,5]). The following section summarizes the test setup and procedures as well as major findings deriving from the series of these experiments.

#### 3.2. Test apparatus and procedures in recent centrifuge experiments

The tests were conducted using two laminar boxes in different

facilities with a centrifugal acceleration of 50g or 25g. Fig. 12 shows typical test setups in the two containers of different sizes. The smaller container shown in Fig. 11(a) had internal dimensions of H300 mm  $\times$  W220 mm  $\times$  L700 mm, while the larger one in Fig. 11(b) had internal dimensions of H600 mm  $\times$  W800 mm  $\times$  L1950 mm. Most of these tests were run with the small container under 50 g using a scaling factor of 50. Some were carried out with the large container under 25 g using a scaling factor of 25. The tests with a scaling factor of 25 simulated proto-type configurations, while those with a scaling factor of 50 was a half scale model of the prototype model. The purpose of using different scaling factors and model sizes was to minimize time and cost involved in this study, while examining the effects of both scaling law and side boundaries of the smaller container located close to the model building. Henceforth, the test apparatus and results presented would be in proto-type scale, except for the characteristics of sands used.

Table 5 summarizes the list of tests considered in this study. Tests A to G were newly conducted for the purpose of this study, while Tests H to P were those previously performed by Tokimatsu et al. [11] and Hino

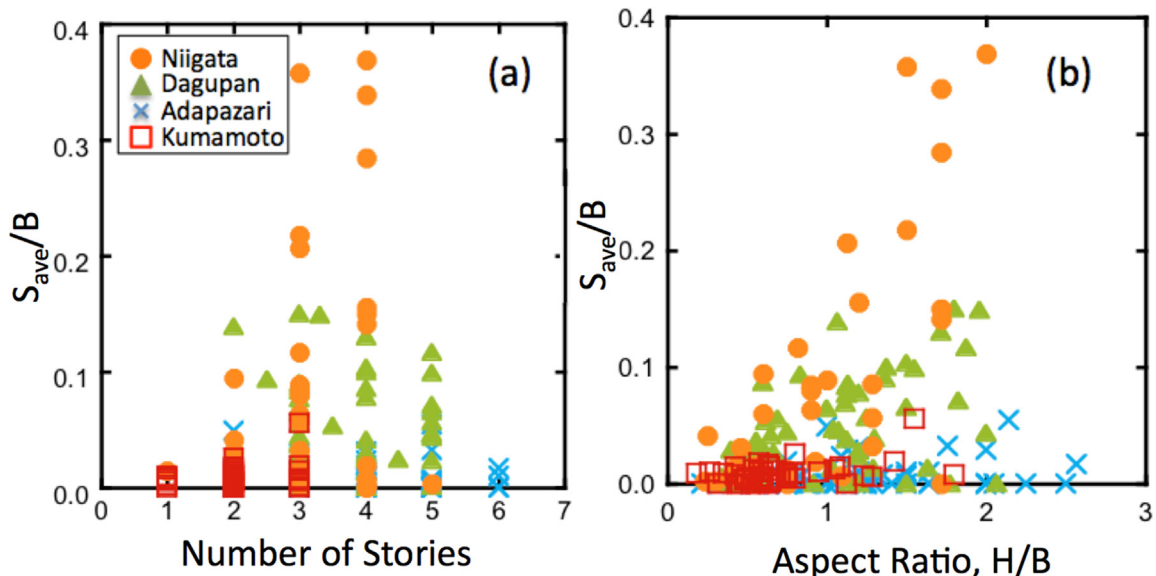


Fig. 8. Relation of settlement-width ratio with number of stories and aspect ratio of building.

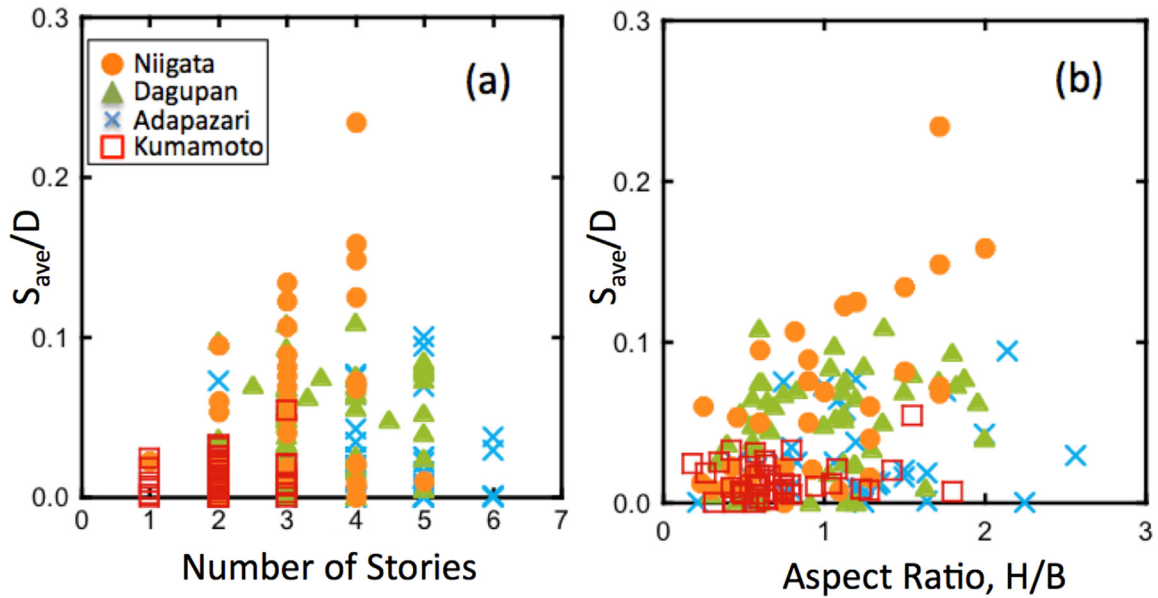


Fig. 9. Relation of settlement-thickness ratio with number of stories and aspect ratio of building.

et al. [5] to investigate the effects of drain pipes on the performance of building. Except for Test E run with a building having a largest base dimension of 9 m, two buildings were laid on liquefiable sand deposits, with the groundwater depth, and soil, building, input ground motion characteristics varied to study their influence. Only one building each is listed for Tests H to P, because drainpipes, which are not the subject of this paper, were installed around the periphery of the other building. A total of 22 buildings with rigid shallow foundations were studied in 16 centrifuge tests.

Table 6 summarizes the characteristics of 8 buildings with different foundation width, contact pressure, height of gravity center, and load eccentricity ratio. The two letters of building ID in turn reflect the contact pressure (2: 20 kN/m<sup>2</sup>; 5: 50 kN/m<sup>2</sup>; 7: 70 kN/m<sup>2</sup>; and 9: 90 kN/m<sup>2</sup>) and foundation width and eccentricity ratio (S: 4.5 m and 0.04; L: 9.0 m and 0.04; L': 8.0 m and 0.04; and E: 4.5 m and 0.10). The natural periods of building were 0.3–0.4 s for 2S, 2L and 2L'; 0.15 s for 5S and 5E; 0.2 s for 7S and 7L; 0.25 s for 9S. The contact pressure, height of gravity center, and natural period of buildings 2S, 2L, and 2L'

correspond to typical two-story wooden houses while the remaining model buildings represent 2- to 4-story RC buildings. The roof floor and foundation of each model building were made of monocast (MC) nylon or duralumin, both of which were tightly affixed to the ends of the column walls made of either MC nylon, ultra super duralumin, or aluminum. The embedded depths of foundation were 0.50 m for Tests A to G, 0.15 m for Tests H to N, and 0.25 m for Tests O and P.

Table 7 summarizes characteristics of 9 model grounds with different groundwater table and different stratification of soil density. The first letter of Soil Model ID reflects groundwater Table (1: 1 m; 2: 2 m, 3: 2.5 m; and 4: 4.0 m), with the rest (one to three letters) representing the variation of relative density (L: 50%; M: 60–65%; and D: 90%) with depth below the groundwater table.

The model ground in Tests A to N was prepared with air-pluviation method in the small laminar box using Silica sand #8 (D<sub>50</sub> = 0.096 mm, e<sub>max</sub> = 1.40, e<sub>min</sub> = 0.78, Non-plastic) at the surface 1 m and Silica sand #7 (D<sub>50</sub> = 0.16 mm, e<sub>max</sub> = 1.18, e<sub>min</sub> = 0.69) below that depth, with silicone oil of 50 cSt as the pore fluid. The coefficient of

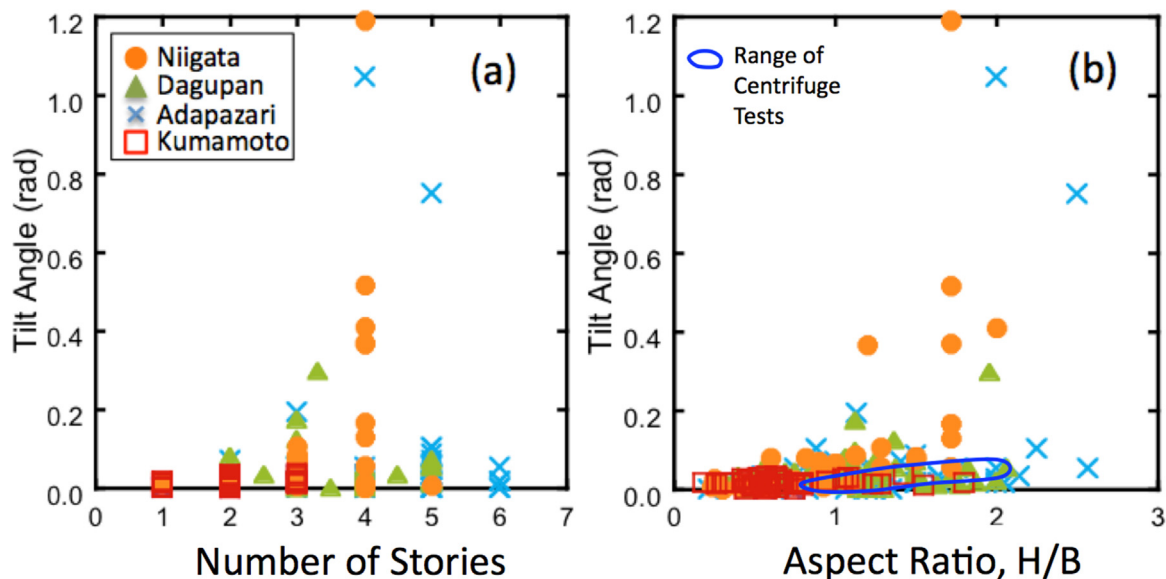
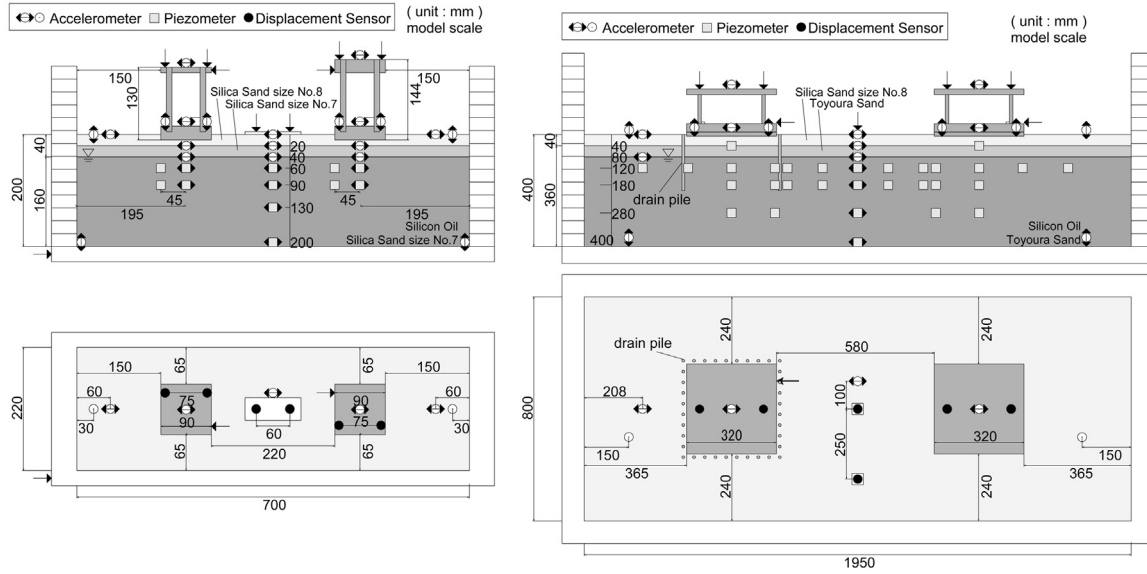


Fig. 10. Relation of tilt angle with number of stories and aspect ratio of building.



(a) Test A

(b) Test O

Fig. 11. Test setups.

**Table 5**  
List of centrifuge tests.

Test ID	Model ID	Build-ing ID	Soil ID	Number of shaking	Centrifugal acceleration
A	5S_2L	5S	2L	5	50G
	7S_2L	7S			
B	5S_3L <sub>2</sub>	5S	3L <sub>2</sub>	6	50G
	7S_3L <sub>2</sub>	7S			
C	5S_4L <sub>2</sub>	5S	4L <sub>2</sub>	6	50G
	7S_4L <sub>2</sub>	7S			
D	5E_3L <sub>2</sub>	5E	3L <sub>2</sub>	4	50G
	9S_3L <sub>2</sub>	9S			
E	7L_3L <sub>2</sub>	7L	3L <sub>2</sub>	5	50G
F	7S_3LD	7S	3LD	4	50G
	9S_3LD	9S			
G	7S_3DL	7S	3DL	8	50G
	9S_3DL	9S			
H	2S_1L	2S	1L	3	50G
I	2S_1L*	2S	1L	2	50G
J	2S_3L	2S	3L	3	50G
K	2S_4L	2S	4L	3	50G
L	2L_1L	2L	1L	2	50G
M	2L_3L	2L	3L	1	50G
N	2L_3L	2L	3L	3	50G
O	2L'_2M	2L'	2M	5	25G
P	2L'_2M'	2L'	2M	3	25G

**Table 6**  
List of building models.

Building ID	Contact pressure (kN/m <sup>2</sup> )	Height of gravity center (m)	Foundation width (m)	Mass eccentric ratio
2S	20	2.5	4.5	0.04
2L	20	2.5	9.0	0.04
2L'	20	2.5	8.0	0.04
5S	50	2.5	4.5	0.04
5E	50	2.5	4.5	0.10
7S	70	3.5	4.5	0.04
7L	70	3.5	9.0	0.04
9S	90	4.5	4.5	0.04

**Table 7**  
List of soil modes.

Soil ID	GWT (m)	Dr (%) above GWT	Dr (%) below GWT
1L	1.0	50	50
3L	2.5	50	50
4L	4.0	50	50
2L	2.0	65	50
2M	2.0	60	60
3L <sub>2</sub>	2.5	65	50
4L <sub>2</sub>	4.0	65	50
3LD	2.5	65	50(2.5–6.5 m)
			90(6.5–10 m)
3DL	2.5	80(0–1.0 m)	90(2.5–6.0 m)
			90(1.0–2.5 m)

permeability of the liquefiable layer below the groundwater table (Silica sand #7) with 50 cSt silicone oil was  $2.8 \times 10^{-4}$  cm/s. The model ground in Tests O and P was made in the large laminar box using Silica sand #8 at the surface of 1 m and Toyoura sand ( $D_{50} = 0.21$  mm,  $e_{max} = 0.99$ ,  $e_{min} = 0.63$ ) below that depth, with silicone oil of 25 cSt as the pore fluid.

In both cases, the sand was saturated with silicone oil under vacuum till the desired groundwater table specified in Table 5. Subsequently, the dry sand layer above the groundwater table was laid with similar air-pluviation means. After completion of sand layer, either one or a pair of building models was placed on the ground with a specified embedment depth. Accelerometers, pore water pressure transducers and displacement meters were installed at specific depths in between the sand pluviation process and on the buildings after placement onto the sand surface.

An artificial ground motion called “Rinkai” [5,11] was used as an input motion in the longitudinal direction of the laminar box. The outputs from the installed sensors were recorded until the excess pore pressure in the ground had dissipated completely. This shaking and observation process was repeated up to several times until the outputs became out of scale. The peak input accelerations were adjusted to  $4.0 \text{ m/s}^2$  for the first flight,  $2.0 \text{ m/s}^2$  for the second flight, and  $4.0 \text{ m/s}^2$  thereafter, for tests A to N. For tests O, peak input accelerations were  $4 \text{ m/s}^2$  for the first three flights and  $7 \text{ m/s}^2$  thereafter. In contrast, accelerations were  $7 \text{ m/s}^2$  for the first two flights and  $8 \text{ m/s}^2$  thereafter for

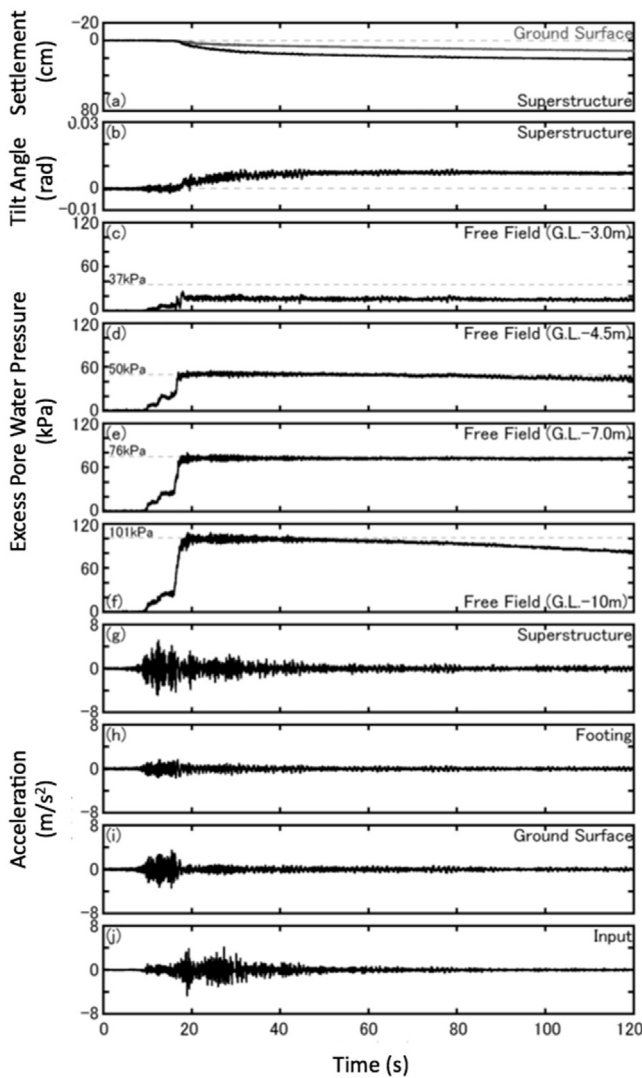


Fig. 12. Major outputs during shaking phase of the first flight of Test P with Model 2L\_2M.

test P. This paper discusses the results from all the flights, while the previous study [12] looked at mainly those from the first flight.

3.3. Effects of contact pressure, soil stratigraphy and intensity of input motions

Fig. 12 shows major outputs during the shaking phase (0–120 s) of the first flight of Test P with Model 2L\_2M. The broken line drawn in each excess pore pressure time history stands for the initial effective stress at the corresponding depth. The excess pore water pressures from

4.5 to 10 m depths become approximately equal to the initial effective stress at 10–18 s, at which the settlement and tilting of building as well as the ground settlement start to occur. About 60–65% of the final settlements of both ground and building occur by the end of shaking (120 s), whereas most (80%) of the final tilt angle takes place during the shaking phase.

The areas encircled in solid lines in Figs. 7(a) and 10(b) correspond to the test results from the centrifuge experiments. The test results are broadly consistent with the lower bound values from field observation, probably due to the difference in in situ soil density and stress history that cannot be mimicked in laboratory tests.

Fig. 13 shows the effect of contact pressure on the absolute settlement, relative settlement, and tilting angle after the excess pore water pressure in the ground had completely dissipated in the first set of flights with soil model 3L2, i.e., the same groundwater table and soil density. Solid circles correspond to the data with the eccentric ratio of 0.04, while solid squares relate to those with a higher eccentric ratio. The solid line in the figure indicates the trend of the results with eccentric ratio of 0.04. The figure confirms that, under the same test conditions, the absolute and relative settlements, and tilting angle of building tend to increase with greater contact pressure. The solid square plotted far above the solid line in Fig. 13(c) also confirms that greater tilt angle of building is resulted from higher eccentricity ratio.

Fig. 14 shows the effect of groundwater table on the absolute and relative settlements, and tilt angle after the first set of flights with building model 7S. The solid symbols connected to the solid line in the figure represent the test results with a homogeneous soil deposit having a relative density of 50%. The figure suggests that, under similar test conditions, the absolute settlement, relative settlement, and tilt angle of building tend to decrease with increasing groundwater table depth. In specific, when groundwater table is as deep as 4 m below the ground surface, the relative settlement and tilting angle of building becomes negligibly small even though the building has suffered absolute settlement arising from soil liquefaction. This infers that the building settled along with the surrounding thick non-liquefied soil layer overlying the liquefied deposit of sand.

The upright triangle in Fig. 14 corresponds to the test with a loose sand layer underlain by a dense sand layer (3LD), while the inverted triangle refers to the test where a dense sand layer was underlain by a loose sand layer (3DL). A comparison of test results with varying density configuration in the figure suggests that the reduction in loose layer thickness immediately below the groundwater table (upright triangle) has minimal effect to the resultant absolute and relative settlement, and tilt angle of building. The increase in non-liquefied layer thickness immediately below the groundwater table, in contrast, does have significant effects on reducing relative settlements of building.

Fig. 15 shows the effect of groundwater table on the absolute settlement, relative settlement, and tilting angle for the first three flights on building model 7S. The extent of settlement and tilting from the second flight ( $2 \text{ m/s}^2$ ) were lower than those observed in the first and third flights with  $4 \text{ m/s}^2$ , suggesting the effects of the peak input accelerations. In addition, the settlement and tilting caused by the third

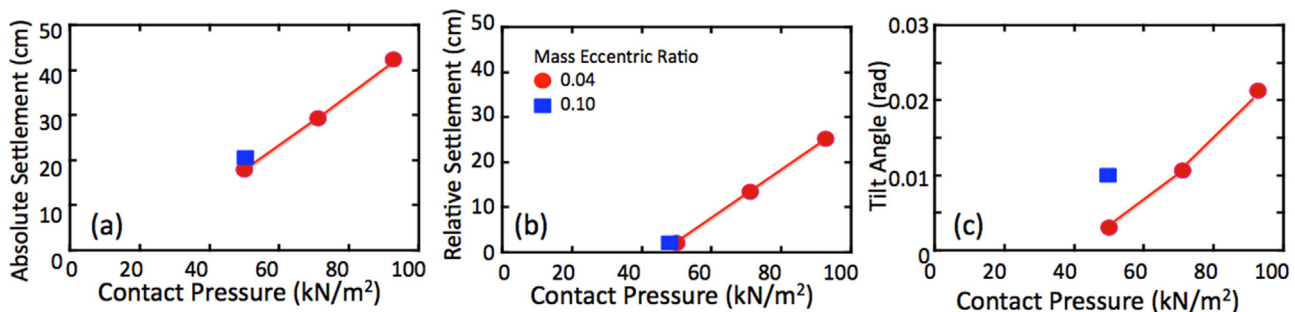


Fig. 13. Effects of contact pressure and mass eccentric ratio on absolute and relative settlement and tilt angle in the first flight with a ground water table of 2.5 m.

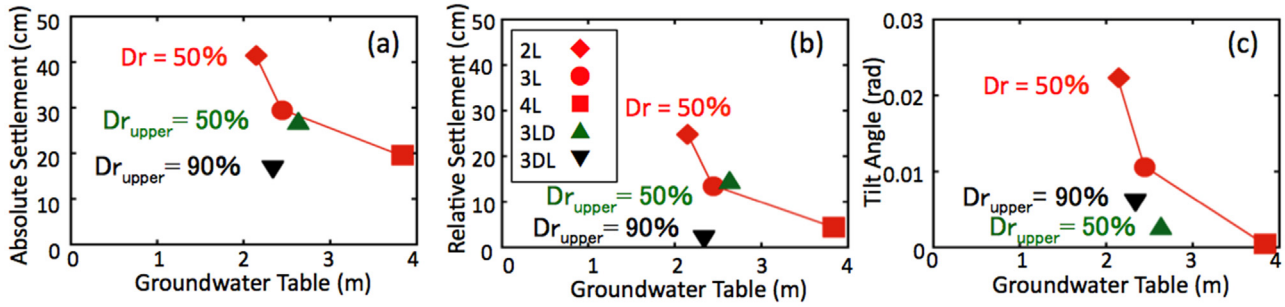


Fig. 14. Effects of groundwater table and soil stratification on absolute and relative settlements and tilting angle of all building models 7S.

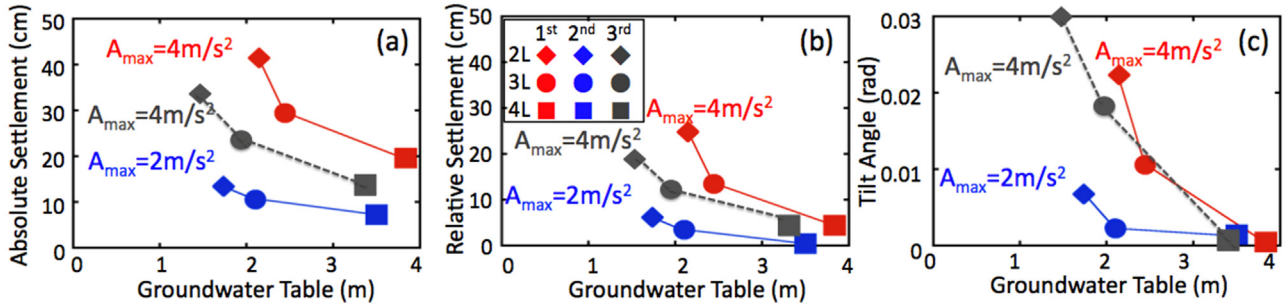


Fig. 15. Effects of groundwater table and input acceleration on absolute and relative settlements and tilt angle in the first, second and third flights with buildings 7S.

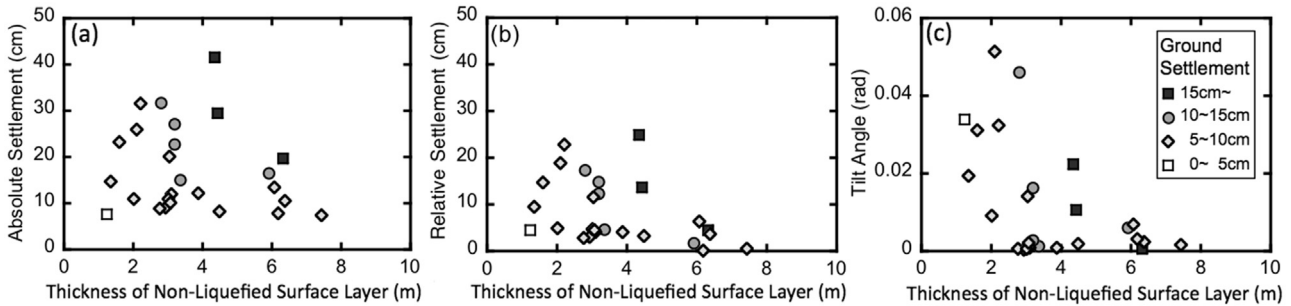


Fig. 16. Relations of the non-liquefied crust thickness with absolute and relative settlements and tilt angle of all building models 7S, in terms of the settlement of level ground.

flight were lower as compare to the first flight, suggesting the effects of soil densification following soil liquefaction during the preceding two flights. Despite soil densification, the tilt angles caused by the third flight are comparable to those of the first flight. This suggests that the reduction in groundwater table depth or the non-liquefied crust thickness might have stronger effects on building tilt.

As observed in Fig. 15, the increase in non-liquefied layer thickness immediately below the building has significant effects on lowering absolute and relative settlements and tilting of building. Fig. 16 thus summarizes the relations of the non-liquefied crust thickness with the absolute and relative settlements and the tilt angle, in terms of liquefaction-induced ground settlement, from all flights and tests with building model 7S. The figure confirms that the increase in non-liquefied near-surface thickness generally decreases settlement and tilting of building and that such a trend becomes significant with decreasing liquefaction-induced settlement of the level ground, i.e., liquefaction severity. This is consistent with the field observations during the 2011 Tohoku earthquakes reported by Tokimatsu et al. [10].

### 3.4. Safety factors against vertical load and overturning moment

In order to evaluate the liquefaction-induced damage to building affected by various key factors in a more scientific manner, Fig. 17

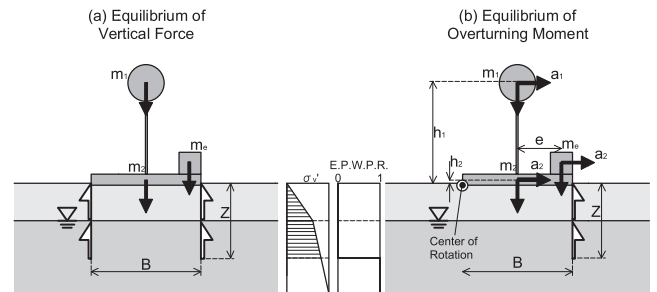


Fig. 17. Equilibrium of vertical force and rotational moment of a building founded on a non-liquefiable layer having of a thickness of Z.

shows the equilibrium of vertical force and rotational moment of a building founded on a non-liquefiable layer having of a thickness of Z. Assuming that only the vertical shear force acting along the perimeter of the building in the non-liquefied crust contributes to the resistance against the vertical force and overturning moment of the building and neglecting the weight of the non-liquefied crust, the safety factor with respect to the vertical force equilibrium  $F_{sw}$  can be represented as

$$F_{sw} = R_w/L_w \quad (1)$$

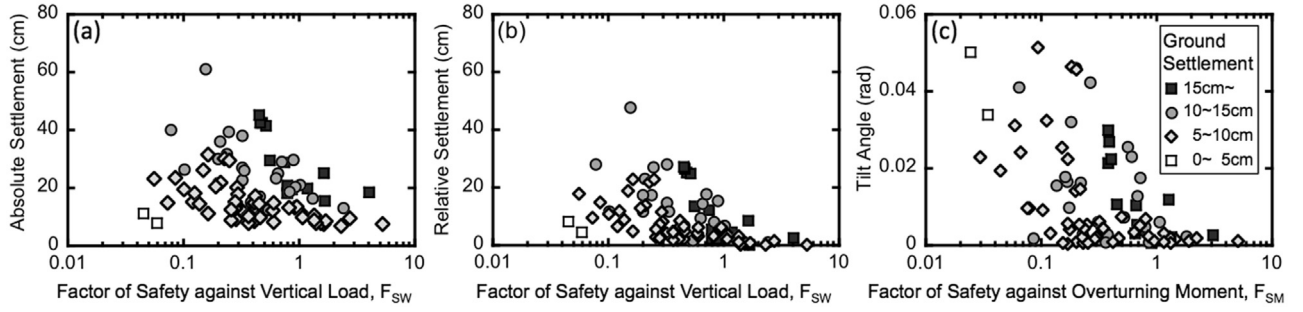


Fig. 18. Relations between safety factor sand absolute and relative settlements and tilt angle of building.

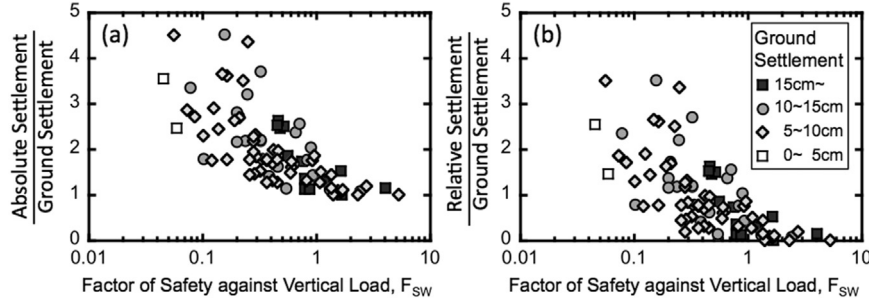


Fig. 19. Relation of safety factor against vertical force with normalized absolute and relative settlements.

in which  $R_w$  is the resisting force and  $L_w$  is the total vertical force of the building; both defined respectively as

$$R_w = \int_0^Z (K\sigma_v' \tan\phi) dz \times (2B + 2L) \quad (2)$$

$$L_w = (m_1 + m_2 + m_e)g \quad (3)$$

in which  $K$  is the coefficient of earth pressure assigned a value of 0.5,  $\sigma_v'$  is the effective vertical stress,  $Z$  is the thickness of the non-liquefied surface layer,  $\phi$  is the internal friction angle of the non-liquefiable soil assigned a value from  $35^\circ$  to  $43^\circ$  for a relative density from 50% to 90%,  $B$  is the building width in the exciting direction,  $L$  is the building length in the orthogonal direction,  $m_1$ ,  $m_2$  and  $m_e$  are the masses of superstructure, foundation and eccentric portion, and  $g$  is the acceleration due to gravity.

The safety factor with respect to the dynamic overturning moment  $F_{SM}$  with respect to the center of rotation shown in Fig. 17 is given as

$$F_{SM} = R_M / L_M \quad (4)$$

in which  $R_M$  is the resisting moment and  $L_M$  is the overturning moment; both defined respectively as

$$R_M = \int_0^Z (K\sigma_v' \tan\phi) dz \times (B + L)B \quad (5)$$

$$L_M = m_1 a_1 h_1 + (m_2 + m_e) a_2 h_2 + (m_1 + m_2) g B / 2 + m_e g (B / 2 + e) \quad (6)$$

in which  $a_1$  and  $a_2$  are the maximum accelerations of the superstructure and foundation upon liquefaction,  $h_1$  and  $h_2$  are the heights of the center of gravity of superstructure and foundation, and  $e$  is the horizontal distance between the centers of the foundation and the eccentric mass.

Fig. 18(a) and (b) show the relationship between the safety factor against vertical force and the absolute and relative settlements from all flights and tests. A well-defined trend exists in which both relative and absolute settlements decrease with increasing factor of safety for a given range of ground settlement. The larger the ground settlement, the larger are the relative and absolute building settlements for a given factor of safety against vertical load. In any case, the relative building settlement becomes negligibly small when the safety factor against vertical force exceeds one.

Fig. 18(c) shows the relationship between the safety factor against dynamic overturning moment and the tilt angle of the building from all flights and tests. The tilt angles of the buildings, although slightly scattered, decreases as the safety factor against overturning moment increases and diminishes to almost zero when it exceeds one.

The relative and absolute settlements shown in Fig. 18 were normalized with respect to ground settlement and plotted in Fig. 19 against their corresponding factors of safety. Both normalized relative and absolute settlements decrease with increasing factor of safety, irrespective of liquefaction-induced ground settlement. The fairly well defined trends in Figs. 18 and 19 suggest that, the safety factors against vertical load and overturning moment, which account for various key parameters pertaining to building, ground and earthquake conditions, are promising and novel indicators to estimate liquefaction-induced damage to buildings founded on rigid shallow foundations.

#### 4. Concluding remarks

The field reconnaissance survey made in Karikusa town, Kumamoto, following the 2016 Kumamoto earthquakes demonstrated that:

- 1) Despite strong ground shaking, liquefaction-induced damage to building in the region was limited within a narrow stretch that was reportedly an old river channel about 400 years ago and later reclaimed artificially.
- 2) Difference in soil behavior within and outside of the liquefied zone was mainly due to the difference in soil type and stratification, i.e., sandy soils with  $I_c < 2$  dominate near the ground surface within, while clayey soils with  $I_c > 2$  prevail outside the liquefied zone.
- 3) The liquefaction-induced relative settlement and tilting of building in the liquefied belt were generally lower than those observed in other earthquakes. This was attributed to the many lightweight wooden houses of 2 stories in the region.
- 4) A few old wooden houses in the liquefied belt experienced damage to their superstructures, owing to their unreinforced weak foundation based on old design specification.

The revisiting of previous earthquake reconnaissance studies on

liquefaction-induced damage to buildings at four sites suggested the following:

- 1) Liquefaction-induced relative settlement and tilting at any site tends to increase with increasing number of stories and aspect ratio of building, but the trend is likely to be site dependent.
- 2) When the settlement was normalized with respect to the thickness of liquefied layer, a general trend exists where increasing number of story and aspect ratio lead to greater normalized settlement, regardless of site-specific conditions.
- 3) Liquefaction-induced overturning of building is dominant only for buildings over 3 stories with aspect ratio greater than about 2.

The centrifuge shaking table tests conducted to investigate the key factors affecting liquefaction-induced damage to buildings with spread foundations suggested the following:

- 1) Liquefaction-induced absolute and relative settlements and tilt angle of building are generally larger with increasing contact pressure and ground settlement, or decreasing groundwater table and thickness of non-liquefied crust. The tilt angle of the building also tends to increase with increasing eccentric mass and distance ratio.
- 2) The safety factors against vertical load and overturning moment are found to be useful indicators to estimate liquefaction-induced damage to building founded on rigid spread foundation.

Since the conclusions drawn from the centrifuge tests are based on a limited set of soil-building conditions and ground motion characteristics, further studies over a wider range of field or test conditions such as duration, frequency content, strong pulse direction of ground motions and interaction between adjacent buildings are recommended to offer a more holistic perspective to improve design of shallow foundations of buildings.

## References

- [1] Architecture Institute of Japan (AIJ). Recommendations for design of small building foundations; 2008. p. 335.
- [2] Cabinet Office, Government of Japan (CAO). Guideline for certifying liquefaction-induced damage to building, action for the Great Tohoku Earthquakes. <[http://www.bousai.go.jp/taisaku/pdf/jiban\\_unyoun.pdf](http://www.bousai.go.jp/taisaku/pdf/jiban_unyoun.pdf)>; 2011.
- [3] Dashti S, Bray JD, Pestana JM, Riemer MR, Wilson D. Mechanisms of seismically-induced settlement of buildings with shallow foundations on liquefiable soil. *J Geotech Geoenviron Eng* 2010;136(1):151–64.
- [4] Gazetas G, Apostolou M, Anastasopoulos J. Seismic bearing capacity failure and overturning of ‘Terveler’ Building in Adapazari, 1999. In: Proceedings of the fifth international conference on case histories in geotechnical engineering. New York, USA; 2004. p. 5.
- [5] Hino K, Tokimatsu K, Suzuki Y, Suzuki H. Effects of groundwater depth on differential settlement of wooden houses during soil liquefaction. In: Proceedings of the Sixth ICEGE. Christchurch, New Zealand; 2015. p. 8.
- [6] Ishihara K. Stability of natural deposits during earthquakes. In: Proceedings of the 11th ICSMFE. Vol. 1; 1985. p. 321–76.
- [7] Okada S, Takai N. Classification of structural types and damage patterns of buildings for earthquake field investigation. *J Struct Constr Eng* 1999;524:65–72.
- [8] Sancio R, Bray JD, Durgunoglu T, Onalp A. Performance of buildings over liquefiable ground in Adapazari, Turkey. In: Proceedings of the 13th world conference on earthquake engineering. Vancouver, Canada, Paper No. 935; 2004.
- [9] Tokimatsu K, Kojima J, Kuwayama S, Abe A, Midorikawa S. Liquefaction-induced damage to buildings in 1990 Luzon Earthquake. *J Geotech Eng* 1994;120(2):290–307.
- [10] Tokimatsu K, Tamura S, Suzuki H, Katsumata K. Building damage associated with geotechnical problems in the 2011 Tohoku Pacific Earthquake. *Soils Found* 2012;52(5):956–74.
- [11] Tokimatsu K, Tohyama K, Suzuki H, Suzuki Y. Experimental investigation on de-watering and drainage methods to mitigate liquefaction damage to existing houses. In: Proceedings of the 10th international conference on urban earthquake engineering. Tokyo, Japan; 2013. p. 543–48.
- [12] Tokimatsu K, Hino K, Ohno K, Tamura S, Suzuki H, Suzuki Y. Liquefaction-induced settlement and tilting of buildings with spread foundation based on field observation and laboratory experiments. In: Proceedings of the 3rd international conference on performance-based design in earthquake geotechnical engineering. Vancouver, B.C., Canada, Paper No. 539; 16–19 July 2017. p. 13.
- [13] Yoshida N, Tokimatsu K, Yasuda S, Kokusho T, Okimura T. Geotechnical aspects of damage in Adapazari City during 1999 Kocaeli, Turkey Earthquake. *Soils Found* 2001;41(4):25–45.
- [14] Yoshimi Y, Tokimatsu K. Settlement of buildings on saturated sand during earthquakes. *Soils Found* 1977;17(1):23–38.